CellPress

Developmental Cell
Article

Profilin-1 Serves as a Gatekeeper for Actin Assembly by Arp2/3-Dependent and -Independent Pathways

Jeremy D. Rotty,[1,2,3,7] Congying Wu,[1,2,3,7] Elizabeth M. Haynes,[1,2] Cristian Suarez,[4] Jonathan D. Winkelman,[4] Heath E. Johnson,[6] Jason M. Haugh,[6] David R. Kovar,[4,5] and James E. Bear[1,2,3,*]
[1]University of North Carolina Lineberger Comprehensive Cancer Center
[2]Department of Cell Biology and Physiology
[3]Howard Hughes Medical Institute
University of North Carolina at Chapel Hill, Chapel Hill, NC 27599, USA
[4]Department of Molecular Genetics and Cell Biology
[5]Department of Biochemistry and Molecular Biology
The University of Chicago, Chicago, IL 60637, USA
[6]Department of Chemical and Biomolecular Engineering, North Carolina State University, Raleigh, NC 27695, USA
[7]Co-first author
*Correspondence: jbear@email.unc.edu
http://dx.doi.org/10.1016/j.devcel.2014.10.026

SUMMARY

Cells contain multiple F-actin assembly pathways, including the Arp2/3 complex, formins, and Ena/VASP, which have largely been analyzed separately. They collectively generate the bulk of F-actin from a common pool of G-actin; however, the interplay and/or competition between these pathways remains poorly understood. Using fibroblast lines derived from an *Arpc2* conditional knockout mouse, we established matched-pair cells with and without the Arp2/3 complex. *Arpc2*$^{-/-}$ cells lack lamellipodia and migrate more slowly than WT cells but have F-actin levels indistinguishable from controls. Actin assembly in *Arpc2*$^{-/-}$ cells was resistant to cytochalasin-D and was highly dependent on profilin-1 and Ena/VASP but not formins. Profilin-1 depletion in WT cells increased F-actin and Arp2/3 complex in lamellipodia. Conversely, addition of exogenous profilin-1 inhibited Arp2/3 complex actin nucleation in vitro and in vivo. Antagonism of the Arp2/3 complex by profilin-1 in cells appears to maintain actin homeostasis by balancing Arp2/3 complex-dependent and -independent actin assembly pathways.

INTRODUCTION

Actin assembly is critical for many cellular processes, including migration, vesicular trafficking, and adhesion (Campellone and Welch, 2010). F-actin can form spontaneously in vitro, but de novo filament nucleation is energetically and kinetically disfavored and requires additional factors to efficiently polymerize both in vitro and in vivo (Campellone and Welch, 2010). The factors responsible for assembling F-actin networks include the Arp2/3 complex, which forms branched actin filaments, and formin and Ena/VASP proteins, which form long, unbranched actin filaments. Each of these classes of actin assembly factors polymerizes F-actin at specific subcellular locations, leading to various cellular responses.

The seven-subunit Arp2/3 complex localizes to endocytic and phagocytic structures, adherens junctions, invadopodia, and the lamellipodia, where it generates the branched actin network under the control of nucleation promoting factors (NPFs) (Rotty et al., 2013). Ena/VASP localizes to the distal tip of the lamellipodium, where it regulates the density and length of Arp2/3 complex-generated branches through its antagonistic relationship with capping protein while also incorporating G-actin to growing barbed ends (Bear et al., 2002; Hansen and Mullins, 2010; Winkelman et al., 2014). However, Ena/VASP proteins also localize to both focal adhesions and filopodia and directly contribute to forming the unbranched, bundled F-actin of the latter (Lanier et al., 1999; Reinhard et al., 1992; Svitkina et al., 2003). Formins are multidomain proteins encoded by 15 distinct genes in mammals that assemble actin in filopodia and stress fibers, and they contribute to lamellipodial dynamics, vesicular transport, cytokinesis, and phagocytosis (Breitsprecher and Goode, 2013). Though much is known about these pathways individually, both in vitro and in cells, we lack a systematic understanding of the collaboration and competition between these pathways in cells.

All of these pathways are thought to share a common pool of G-actin, which must be divided among distinct F-actin assembly factors at various subcellular locations (Chesarone and Goode, 2009; Gao and Bretscher, 2008). In yeast, which lack Ena/VASP proteins and have only two (budding yeast) or three formins (fission yeast), the Arp2/3 complex is known to generate actin patches involved in endocytosis (Winter et al., 1999), while formin isoforms generate a completely distinct network of actin cables that polarize cells for division and form the contractile ring (Evangelista et al., 2002; Sagot et al., 2002). Recent studies revealed that inhibition of the Arp2/3 complex leads to compensatory F-actin assembly by formins in fission yeast (Burke et al., 2014). Arp2/3 complex-dependent and -independent assembly pathways show a similar compensation in mammalian cells,

although the mechanism remained obscure until now (Hotulainen and Lappalainen, 2006; Steffen et al., 2006; Suraneni et al., 2012; Wu et al., 2012).

Here, we report a detailed analysis of the F-actin network structure, dynamics, and content of fibroblasts genetically null for the p34 subunit of the Arp2/3 complex. We find that Ena/VASP and profilin maintain F-actin levels in the absence of Arp2/3 complex function in mammalian cells. We also find evidence for an inhibitory relationship between profilin and the Arp2/3 complex. Our findings in mouse fibroblasts, together with the work of Suarez et al. (2015) in this issue of *Developmental Cell*, which uses fission yeast and in vitro single-molecule imaging techniques, suggest that profilin preferentially delivers actin monomers to Ena/VASP and formin pathways and inhibits Arp2/3 complex-based nucleation. The profilin-dependent interplay between these pathways creates a homeostatic balance that allows each pathway to function side by side in a common cytoplasmic compartment in order to drive higher order cellular processes like lamellipodial protrusion, endocytosis, and cell division that depend on complex and varied actin networks.

RESULTS

Generation and Characterization of *Arpc2*$^{-/-}$ Fibroblast Lines

Based on our recent finding that cells depleted of Arp2/3 complex by RNAi are viable in the *Ink4a/Arf*$^{-/-}$ genetic background and proliferate in culture (Wu et al., 2012), we crossed mice containing a conditional *Arpc2* allele (consisting of LoxP sites flanking exon 8 of the gene encoding the p34 subunit of the Arp2/3 complex) into the *Ink4a/Arf*$^{-/-}$ background. Cells derived from these mice lack both Arf and p16^{INK4a} and proliferate readily in culture before and after the deletion of the *Arpc2* gene. Fibroblasts were isolated from both embryonic (mouse embryonic fibroblasts [MEFs]) and adult tail (mouse tail fibroblasts [MTFs]) tissue of these mice, stably transduced with CreER, and grown up as clonal lines. Based on initial validation of multiple clonal lines, we proceeded with one MEF line (MEF 10-4) and one MTF line (MTF24) for subsequent experiments. Treatment of clonal lines with tamoxifen (4-OHT) to activate the Cre recombinase activity generated matched pair cell lines with and without the complete loss of p34 protein (referred to as *Arpc2*$^{-/-}$ and wild-type [WT] throughout) and led to the loss of other Arp2/3 complex subunits as well (Figures 1A and 1B). These *Arpc2*$^{-/-}$ lines lack lamellipodia and are dominated instead by filopodial protrusions; they contain abundant stress fibers as well (Figure 1C; Figure S1A available online). Stable reintroduction of p34-GFP via lentivirus restored Arp2/3 complex protein levels and lamellipodia (Figures 1D and 1E). Both *Arpc2*$^{-/-}$ lines showed severe defects in single cell motility that were rescued by the reintroduction of p34-GFP (Figure 1F).

Loss of Arp2/3 Complex Affects F-Actin Structure and Dynamics, but Not Total F-Actin Levels

The genetic ablation of Arp2/3 complex in mammalian fibroblasts provides an opportunity to analyze the actin cytoskeleton in the absence of one of its major regulators. Actin filaments are considerably less dynamic in *Arpc2*$^{-/-}$ cells than WT controls as shown by imaging the actin probe LifeAct (LA), leading to less dynamic protrusion and retraction (Figure 2A; Figure S1B; Movies S1 and S2), consistent with their slow migration. We used cryo-shadowing electron microscopy (EM) (Wu et al., 2012) to confirm the absence of a dense network of lamellipodial actin in *Arpc2*$^{-/-}$ cells with F-actin organized instead into parallel bundles of actin within filopodial protrusions (Figure 2B). Although the organization of F-actin is strikingly different in these cells, we tested whether the balance of F- versus G-actin was affected by the loss of Arp2/3 complex.

Total F-actin levels were analyzed with fluorescent phalloidin in fixed cells plated in mixed populations (i.e., WT and *Arpc2*$^{-/-}$ cells plated side by side; Figure S1C). Low-magnification epifluorescent imaging captured fluorescent signal from all focal planes, and integrated pixel density of phalloidin fluorescence was used to calculate relative F-actin content. Whole cell lysates of matched cell numbers were prepared to analyze total actin levels via immunoblot. WT and *Arpc2*$^{-/-}$ cells had similar levels of total actin and, surprisingly, similar levels of F-actin (Figures 2C and 2D; Figure S1C). Thus, other polymerization mechanisms compensate for loss of Arp2/3 complex activity and maintain actin filament levels.

Both WT and *Arpc2*$^{-/-}$ F-actin was equally susceptible to 500 nM latrunculin B (LatB) (Figure S1D), but F-actin in *Arpc2*$^{-/-}$ lines was more resistant to 100 nM cytochalasin D (CD) than WT cells when examined side by side (Figure 2E; Figure S1E). Furthermore, WT cell motility was significantly reduced by CD, while *Arpc2*$^{-/-}$ cell motility was either not affected by the drug or enhanced, depending on the cell line (Figure 2F; confirmed in Arp2/3 complex-depleted 2xKD cells in Figure S1F). LatB predominately sequesters actin monomers (Spector et al., 1989) while 100 nM CD predominantly binds actin filament barbed ends rather than actin monomers (Cooper, 1987). Thus, actin polymerization in cells without Arp2/3 complex depends on actin assembly factors that are resistant to CD and generate unbranched actin filaments.

Actin Assembly in *Arpc2*$^{-/-}$ Cells Is Profilin-1 Dependent

Based on the difference in susceptibility to the barbed-end toxin CD, we used barbed-end labeling assays to localize and quantify actin assembly in situ using labeled actin monomers in cells with or without Arp2/3 complex (Symons and Mitchison, 1991). To our surprise, monomer incorporation in both *Arpc2*$^{-/-}$ and Arp2/3 complex-depleted 2xKD cells was reduced compared to control cells (Figures 3A and 3B; Figure S2A). Several non-Arp2/3 complex-based actin assembly pathways preferentially utilize profilin-actin complexes (Hansen and Mullins, 2010; Romero et al., 2004), and transcriptome profiling indicates that profilin-1 is, by far, the dominant profilin isoform expressed in fibroblasts (>100-fold at the mRNA level than profilin-2) (Wu et al., 2013). Therefore, we repeated the barbed-end incorporation with a mixture of labeled actin and purified profilin-1 and found that the presence of profilin rescued actin monomer incorporation in *Arpc2*$^{-/-}$ and 2xKD cells (Figures 3A and 3B; Figure S2A). Interestingly, barbed-end labeling of WT cells was reduced overall (Figure 3B), as well as being significantly reduced at the leading edge (Figure 3C) in the presence of profilin-1. Based on these data, we postulated that *Arpc2*$^{-/-}$ cells would be more sensitive to the loss of profilin-1 than WT cells.

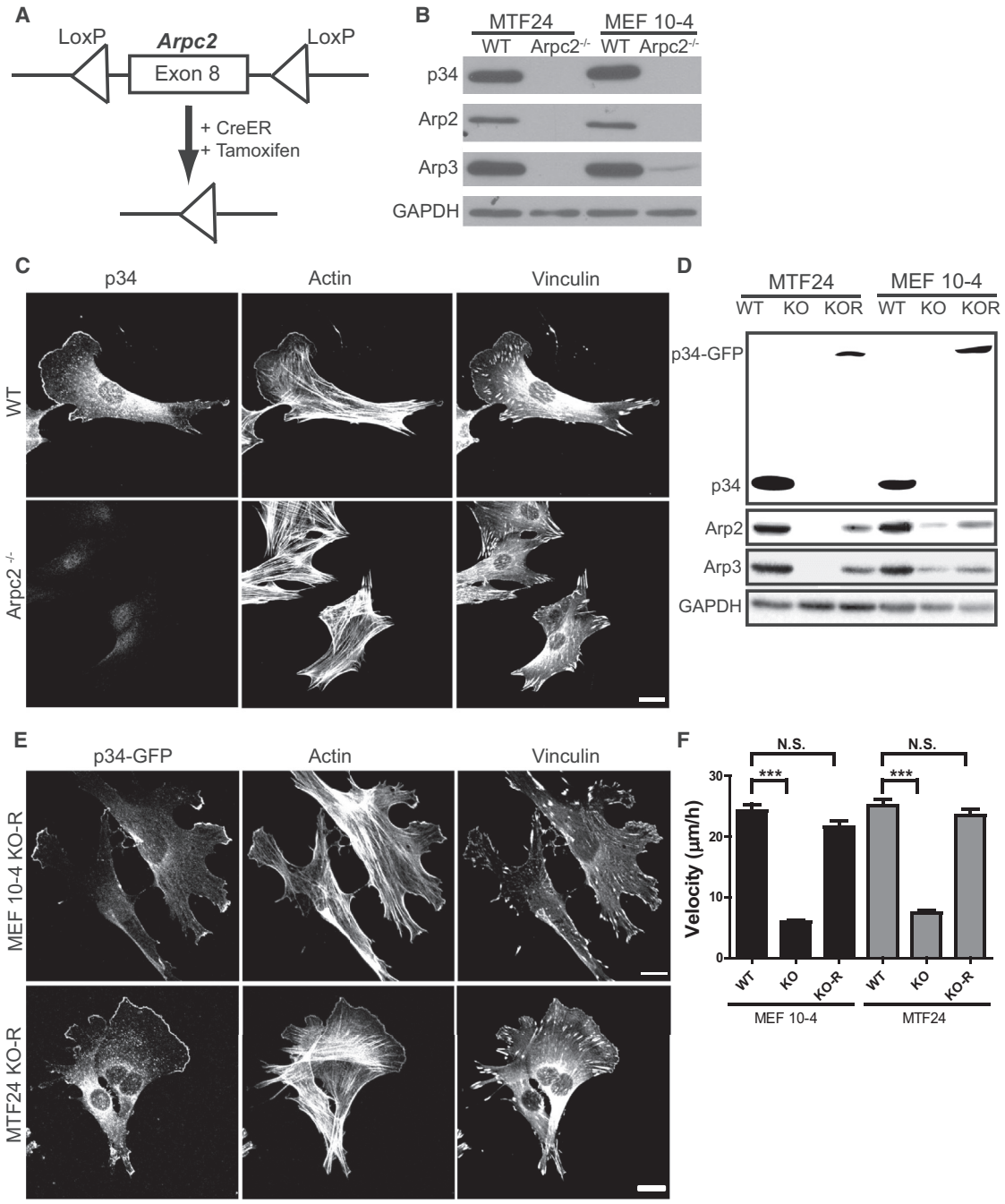

Figure 1. Generation and Characterization of *Arpc2*$^{-/-}$ Fibroblast Cell Lines

(A) Schematic representation of tamoxifen-inducible CreER activation and *Arpc2* (p34) deletion.

(B) Blot analysis of two mouse fibroblast cell lines without (WT) or with (*Arpc2*$^{-/-}$) tamoxifen treatment.

(C) Staining of MTF24 WT and *Arpc2*$^{-/-}$ fibroblasts. Scale bar, 20 μm.

(D) Blot analysis of cell lines without (WT) or with (KO) tamoxifen treatment or KO cells stably rescued with p34-GFP (KOR).

(E) Staining of MEF 10-4 KOR and MTF24 KOR fibroblasts; GFP indicates p34-GFP. Scale bars, 20 μm.

(F) Random migration velocity of WT, KO, and KOR MEF 10-4 (black bars) and MTF24 (gray bars) fibroblasts; N = at least 54 cells per condition; error bars represent SEM; ***$p < 0.0001$. N.S., not significant.

See also Figure S1.

Consistent with our hypothesis, depletion of profilin-1 in *Arpc2*$^{-/-}$ cells (via two distinct small hairpin RNAs [shRNAs]) leads to decreased F-actin levels (Figures 3D and 3E; Figures S2B–S2D). These *Arpc2*$^{-/-}$, profilin-depleted cells have a severely compromised ability to spread and highly disorganized F-actin, with a decrease in the appearance and length of

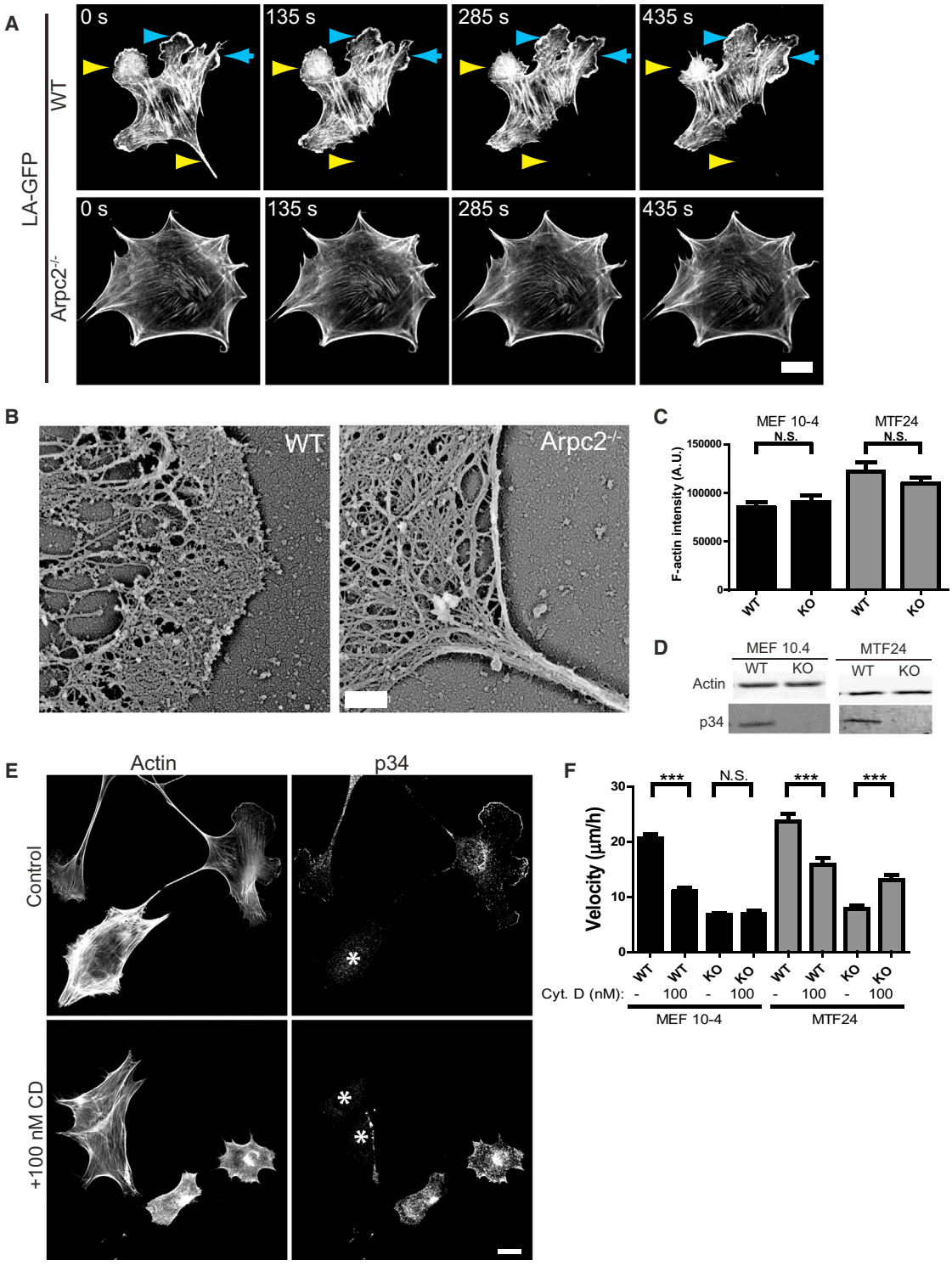

Figure 2. Comparison of Actin Structure and Dynamics in WT and *Arpc2*$^{-/-}$ Cells

(A) Still frames from live cell imaging of MEF 10-4 WT and *Arpc2*$^{-/-}$ cells stably transfected with the live cell actin probe LA-GFP showing dynamic F-actin behavior in each cell type. Cyan arrowheads denote protrusion, yellow arrowheads denote retraction. Scale bar, 20 μm.

(B) Cryoshadowing EM of F-actin networks in MTF24 WT and *Arpc2*$^{-/-}$ cellular protrusions. Scale bar, 500 nm.

(C) Integrated pixel density of phalloidin staining in fixed WT and KO cells from both lines plotted as average F-actin intensity per cell. N = 100 cells per condition; error bars represent SEM; N.S., not significant. A.U., arbitrary units.

(D) Blots of whole cell lysates loaded by cell equivalents for both lines.

(legend continued on next page)

filopodia (Figure 3D; Figures S2C and S2E). These data confirm that compensatory actin assembly in *Arpc2*$^{-/-}$ cells requires profilin-bound actin monomers.

Profilin-1 Inhibits Arp2/3 Complex Function

Based on our in situ cell staining results with profilin-1, we hypothesized that its depletion would lead to cellular effects consistent with enhanced Arp2/3 complex activity. Indeed, depletion of profilin-1 in cells with intact Arp2/3 complex (WT) leads to strikingly different effects than depletion in *Arpc2*$^{-/-}$ cells. In WT cells, profilin-1 depletion led to increased levels of F-actin (Figures 3E and S2D) and alterations in cell morphology and actin organization (Figures 3D and S2C). WT cells depleted of profilin-1 have broad lamellipodia that contain abundant Arp2/3 complex (Figures 3D and S2C). These cells have increased actin arcs, bundled actin structures that run parallel to the cell edge that are known to be Arp2/3 complex derived (Figures 3D and S2C) (Hotulainen and Lappalainen, 2006). Unlike *Arpc2*$^{-/-}$ cells depleted of profilin-1, these cells had increased spread area relative to controls (Figure S2E). To quantify the changes in Arp2/3 complex distribution in the WT (Arp2/3^{+}), profilin-depleted cells, we used previously established edge-mapping techniques (Cai et al., 2007). The width of both the Arp2/3 complex and F-actin bands at the cell periphery is significantly increased in profilin-1-depleted cells (Figure 3F). Furthermore, a greater fraction of the cell edge is positive for Arp2/3 complex, and the average peripheral length of lamellipodia is greater in profilin-1-depleted cells compared to WT controls (Figures 3G, 3H, S3A, and S3B). Profilin-1 depletion enhances Arp2/3 complex localization to the leading edge, broadens the lamellipodial F-actin band, and increases lamellipodia size, suggesting enhanced branch nucleation. These findings led us to directly test whether profilin-1 inhibits Arp2/3 complex branch nucleation.

We used in vitro total internal reflection fluorescence (TIRF) microscopy-based actin polymerization assays to revisit the observation that profilin inhibits Arp2/3 complex nucleation in vitro (Machesky et al., 1999). We found that profilin-1 inhibits Arp2/3 complex branch generation ~6-fold (Figures 4A and 4B). We utilized profilin-1 mutants to further probe the underlying mechanism. The inhibitory activity of profilin-1 is dependent on its ability to bind to actin monomers, as the G-actin binding mutant (R88E) has no inhibitory effect. Conversely, the polyproline binding mutant (Y6D) inhibits Arp2/3 complex-dependent branch formation comparably to WT profilin-1.

To test the inhibitory effect of profilin-1 on Arp2/3 complex activity in cells, we performed the counterexperiment to our profilin-depletion studies by elevating profilin levels. We were unable to achieve satisfactory genetic profilin-1 overexpression in our lines, so instead we turned to profilin-1 microinjection to directly test for an inhibitory effect on Arp2/3 complex function. Precedence exists in the literature for disruption of lamellipodia after profilin microinjection (Cao et al., 1992), but these observations were limited to morphological analysis and did not include an investigation of the molecular processes involved. For our experiments, we used our *Arpc2*$^{-/-}$ p34-GFP rescue line, which also stably expressed LA-red fluorescent protein (RFP) to monitor both Arp2/3 complex and F-actin in the same cell before and after microinjection of ~0.5 pl of 2 mg/ml (133 μM) human profilin-1. Although the precise volume injected and the starting volume of the cell vary by ~2-fold, this corresponds approximately to a step increase in cytoplasmic profilin-1 concentration from 29 μM to 39 μM, or 36% (see Experimental Procedures). Cy5-dextran was used in the mixture to mark injected cells (Figure S3C). Preinjection images (0 min) were taken immediately before microinjection, after which the saved stage positions were revisited and imaged cells were microinjected. The exact time that postinjection images were acquired varied slightly from experiment to experiment based on the length of time required for microinjection. Buffer-alone-injected cells typically maintained lamellipodia and Arp2/3 complex localization at the periphery, whereas microinjection of 2 mg/ml WT profilin led to acute and persistent disruption of Arp2/3 complex edge localization and the disappearance of lamellipodia (Figure 4C). To test the requirement for G-actin binding by profilin in this response, we microinjected R88E mutant profilin-1, which failed to inhibit the Arp2/3 complex in our TIRF experiments. With this mutant profilin-1, we observed an intermediate phenotype with cells retaining some peripheral Arp2/3 localization and morphological lamellipodia, albeit to a reduced extent relative to buffer-alone injections (Figure 4C). Unfortunately, the Y6D mutant profilin-1 proved unsuitable for microinjection due to needle clogging. To quantify the effects of profilin microinjection, we measured the percentage of p34-positive edge and the average length of lamellipodia before and after microinjection, and we measured changes consistent with our visual impressions (Figures 4D and 4E). These data suggest that profilin antagonizes the Arp2/3 complex and that its ability to bind G-actin plays a significant role in this activity.

In addition to the Arp2/3 complex, we concomitantly observed the F-actin network via LA-RFP labeling in these cells. At early time points after WT profilin microinjection, the F-actin network was disrupted in protrusive lamellipodia, as well as in stress fibers, while cells responded later by repolymerizing actin into stress fibers but not lamellipodia (Figure 5A, quantified as shown in Figure S3D). Neither buffer- nor R88E-injected cells demonstrated the same level of F-actin disruption (Figure 5A), suggesting that actin monomer binding was important for WT profilin's acute effect on F-actin. We tested whether *Arpc2*$^{-/-}$ cells expressing LA-RFP were similarly affected by WT profilin. In these cells, we saw no significant disruption of F-actin in *Arpc2*$^{-/-}$ cells, regardless of microinjection condition (Figure 5B), aside from a modest effect with R88E profilin reflecting a possible dominant-negative effect toward endogenous profilin-dependent pathways. The *Arpc2*$^{-/-}$ cells generate no F-actin via the Arp2/3 complex, are highly dependent upon profilin for maintaining F-actin homeostasis (Figure 3E; Figure S2D), and are much less dynamic than WT cells (Figure 1F; Figure 2A),

(E) Staining of MTF24 WT and *Arpc2*$^{-/-}$ fibroblasts in mixed culture (KO cells marked with an asterisk) after addition of 100 nM CD for 2 hr. Scale bar, 20 μm.
(F) Random migration velocity of MEF 10-4 (black bars) and MTF24 (gray bars) WT and KO control (−) cells or cells treated with 100 nM CD (Cyt. D) (+); N = at least 30 cells per condition; error bars represent SEM. ***$p \leq 0.0001$. h, hours.
See also Figure S1.

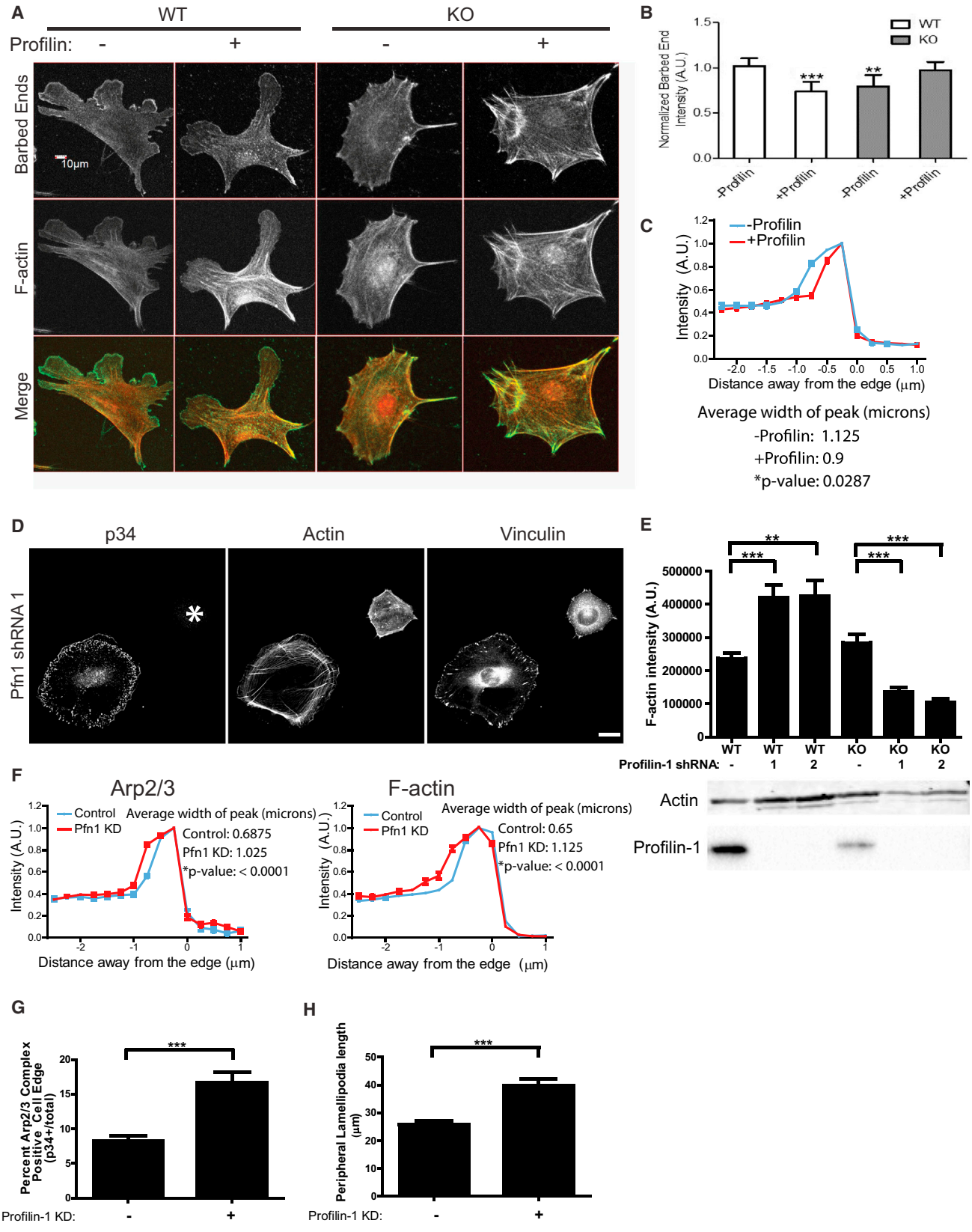

(legend on next page)

leading to lower levels of filament turnover and less free G-actin available for profilin binding. These factors together likely contribute to *Arpc2*$^{-/-}$ resistance to exogenous profilin.

Ena/VASP Proteins, but Not Formins, Maintain *Arpc2*$^{-/-}$ F-Actin Levels

We assessed the contribution of formins to the F-actin network in WT and *Arpc2*$^{-/-}$ cells. Formins are profilin-dependent actin assembly factors that nucleate actin filaments and increase the F-actin barbed-end elongation rate up to 10-fold (Kovar et al., 2006). The mammalian formin family contains isoforms encoded by 15 genes, of which 11 are expressed in mouse fibroblasts (Wu et al., 2013). Since all formins contain an FH2 domain, we used the recently characterized formin inhibitor SMIFH2 that directly inhibits the FH2 domain (Rizvi et al., 2009) and should act as a panformin inhibitor, although the drug's efficacy toward every member of the formin family has not been carefully tested. WT cell motility is decreased by SMIFH2, while *Arpc2*$^{-/-}$ cell motility is unaffected or slightly enhanced by the drug, depending on the cell line (Figure 6A). F-actin levels are not significantly altered in WT cells treated with 15 μM SMIFH2 compared to untreated controls (Figure 6B); and cells retain lamellipodia and stress fiber staining in the presence of the drug (Figures S4A and S4B). Surprisingly, *Arpc2*$^{-/-}$ cells are largely resistant to the effects of SMIFH2 as measured by F-actin levels, and F-actin organization does not significantly differ from untreated *Arpc2*$^{-/-}$ cells (Figure 6B; Figures S4A and S4B). Together, these data indicate that formins clearly contribute to generating F-actin for cell motility in cells with Arp2/3 complex but may not be as important in the absence of Arp2/3 complex, at least in mammalian cells.

Ena/VASP proteins are profilin-binding, actin assembly proteins that bind to the barbed ends of actin filaments, block capping protein binding, and enhance barbed-end growth (Bear et al., 2002; Hansen and Mullins, 2010; Winkelman et al., 2014). Profilin-1 hemizygous mice bred into a *Mena*$^{-/-}$ genetic background die in utero due to severe neurulation defects, indicating dosage-dependent genetic interactions (Lanier et al., 1999). A puzzling aspect of Ena/VASP function is its inhibition of Arp2/3 complex branching in favor of filament elongation or "antibranching" (Bear et al., 2002; Skoble et al., 2001). TIRF microscopy assays using mammalian proteins reveal that VASP alone is not sufficient to block Arp2/3 complex nucleation (Figure S5A). However, inclusion of profilin in the reaction led to a significant decrease in actin branches (Figures S5A and S5B). Control experiments reveal that VASP was active in these assay conditions, as it was able to enhance the elongation rate of actin filaments ~2-fold (Figure S5C). These data argue that the "antibranching" effect observed in previous studies may be due to preferential usage of profilin-actin by Ena/VASP proteins to elongate rather than nucleate actin filaments.

We tested the role that Ena/VASP proteins play in the actin assembly occurring in the *Arpc2*$^{-/-}$ cells. Interestingly, both VASP and Mena are overexpressed in our *Arpc2*$^{-/-}$ cell lines relative to their WT counterparts (Figure 6C; 4-fold for VASP and 1.74-fold for Mena on average). The staining pattern of VASP and Mena in WT cells is consistent with the known localization of Ena/VASP proteins to lamellipodia, focal adhesions, and filopodial tips (Figure 6D). In *Arpc2*$^{-/-}$ cells, VASP and Mena localize to filopodial tips and to focal adhesions that form at the base of these filopodia (Figure 6D, and insets), which is similar to the barbed-end staining pattern in *Arpc2*$^{-/-}$ cells incubated with profilin (Figure 3A). Depletion of profilin-1 does not affect VASP localization in cells with intact Arp2/3 complex; however, in the absence of Arp2/3 complex and depletion of profilin-1, VASP is largely restricted to small focal adhesions at the periphery (Figure S5D). To functionally address the role of Ena/VASP proteins in Arp2/3 complex-independent actin assembly and homeostasis, we stably transduced WT or *Arpc2*$^{-/-}$ cells with a previously characterized dominant interfering construct (termed GFP-FP4-mito, or FP4-mito) that sequesters all Ena/VASP family proteins to mitochondria (Figure S5E) (Bear et al., 2000). Disruption of Ena/VASP activity in WT fibroblasts (via FP4-mito expression or genetic null lines) alters actin organization in lamellipodia and enhances cell motility but does not block lamellipodia generation (Bear et al., 2000). As expected, total F-actin levels are unchanged in WT (Arp2/3^{+}) FP4-mito cells (Figures 6E and 6F; Figures S6A–S6C). However, the combination of Arp2/3 complex deficiency and Ena/VASP sequestration significantly decreases spread cell area and reduces cellular protrusions (i.e., bundled filopodia of *Arpc2*$^{-/-}$ cells) (Figures 6E and 6G; Figures S6A and S6D), as well as overall F-actin levels (Figure 6F; Figure S6C). Thus, compromising Ena/VASP activity in *Arpc2*$^{-/-}$ cells phenocopies

Figure 3. Actin Assembly in *Arpc2*$^{-/-}$ Cells Is Highly Dependent on Profilin

(A) Barbed-end assay relating the distribution of labeled barbed ends to total F-actin in MEF 10-4 WT or KO cells in the absence (−) or presence (+) of profilin. Scale bar, 10 μm.

(B) Quantification of barbed-end staining. Barbed-end fluorescence intensity normalized to F-actin, with each condition plotted relative to control cells (WT minus profilin). Data are plotted as mean and 95% confidence interval. **p = 0.0036; ***p = 0.0001. A.U., arbitrary units.

(C) Barbed-end distribution at the periphery of WT MEF 10-4 cells in the presence (+) or absence (−) of profilin in barbed-end assay (cell edge = 0, negative values = intracellular distance from edge). Plotted as mean ± SEM. The mean width of the peak intensity was also quantified and analyzed by t test and is presented numerically alongside the graph.

(D) Staining of MEF 10-4 WT and *Arpc2*$^{-/-}$ profilin-1 KD fibroblasts (Pfn1 KD) in mixed culture (KO cell marked with an asterisk). Scale bar, 20 μm.

(E) Integrated pixel density of phalloidin staining in fixed MEF 10-4 WT and KO cells ± Pfn1 KD plotted as average F-actin intensity per cell, with SEM. N = 50 cells per condition. **p = 0.0003; ***p < 0.0001. Blots of whole cell lysate matched by cell number appear directly below.

(F) Distribution of p34 and F-actin at the periphery of control or Pfn1 KD MEF 10-4 cells (cell edge = 0, negative values = intracellular distance from edge). Plotted as mean ± SEM. The mean width of the peak intensity was also quantified and analyzed by t test and is presented numerically alongside the graph.

(G) Comparison of Arp2/3-positive edge in MEF 10-4 control or Pfn1 KD cells. High Arp2/3 complex signal in a narrow band along the perimeter was detected and divided by total cell perimeter to yield Arp2/3 complex-enriched edge, plotted as average percent Arp2/3 complex-positive edge with SEM. N = 29 for WT and 24 for WT Pfn1 KD cells. ***p < 0.0001.

(H) Peripheral lamellipodia length. The length of p34-positive edge was determined by outlining the periphery of each protrusion in ImageJ to yield the peripheral length in microns. N = at least 128 lamellipodia. Data are plotted as mean ± SEM. ***p < 0.0001.

See also Figures S2 and S3.

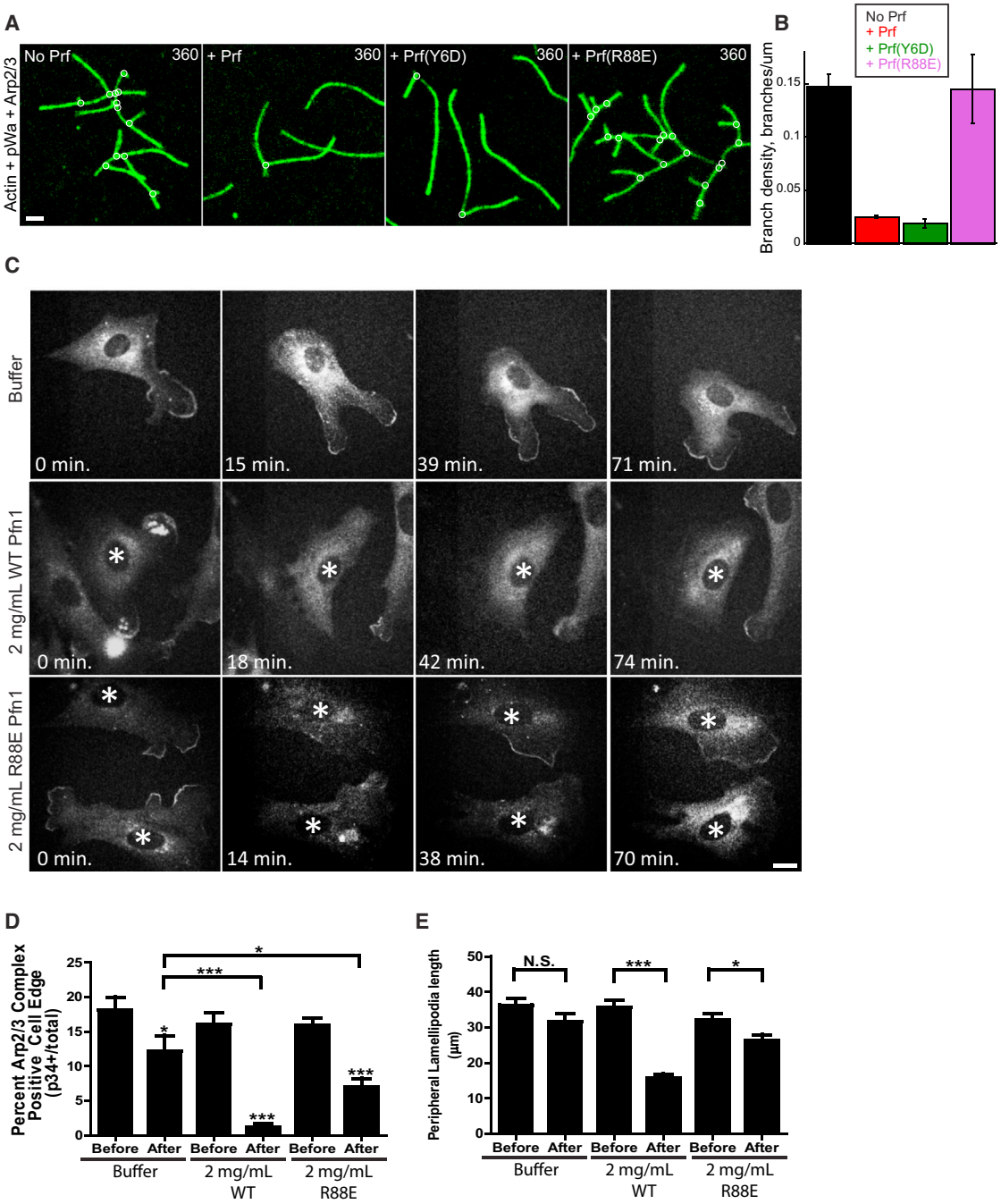

Figure 4. Profilin Inhibits Arp2/3 Complex Actin Nucleation, Disrupts Arp2/3 Complex Leading Edge Localization, and Impedes Lamellipodia Generation

(A) Time-lapse TIRF microscopy of 1.5 μM Oregon green-labeled actin polymerized in the presence of 40 nM Arp2/3 complex, 150 nM pWA in the absence (No Prf) or presence of either 5 μM WT (+ Prf), Y6D, or R88E hProfilin-1. Scale bar, 2 μm.

(B) Effect of WT, Y6D, or R88E hProfilin-1 on branch density, quantified from time-lapse TIRF experiments in (A). Plotted as mean plus SEM.

(C) Representative images of p34-GFP localization before (0 min) and at various times after microinjection of buffer, 2 mg/ml WT hProfilin-1, or 2 mg/ml R88E hProfilin-1. Scale bar, 20 μm. Asterisks denote microinjected cells in images with multiple cells.

(D) Percentage of p34-GFP-positive edge. Quantified as positive edge/total edge × 100% based on measurements done by hand in ImageJ. Measurements were made before and directly after microinjection for each condition, plotted as mean with SEM. N = at least 31 cells per condition. *$p < 0.05$; ***$p < 0.0001$; p values for each postinjection mean are to preinjected cells of same condition, unless explicitly noted otherwise.

(E) Peripheral lamellipodia length. The length of p34-GFP-positive edge was determined by outlining the periphery of each protrusion in ImageJ to yield the peripheral length in microns, plotted as mean with SEM. N = at least 66 lamellipodia in preinjection for each condition; N = 67 for buffer postinjection, 58 for R88E postinjection, and 11 for WT postinjection. *$p = 0.0426$; ***$p = 0.0006$.

See also Figure S3.

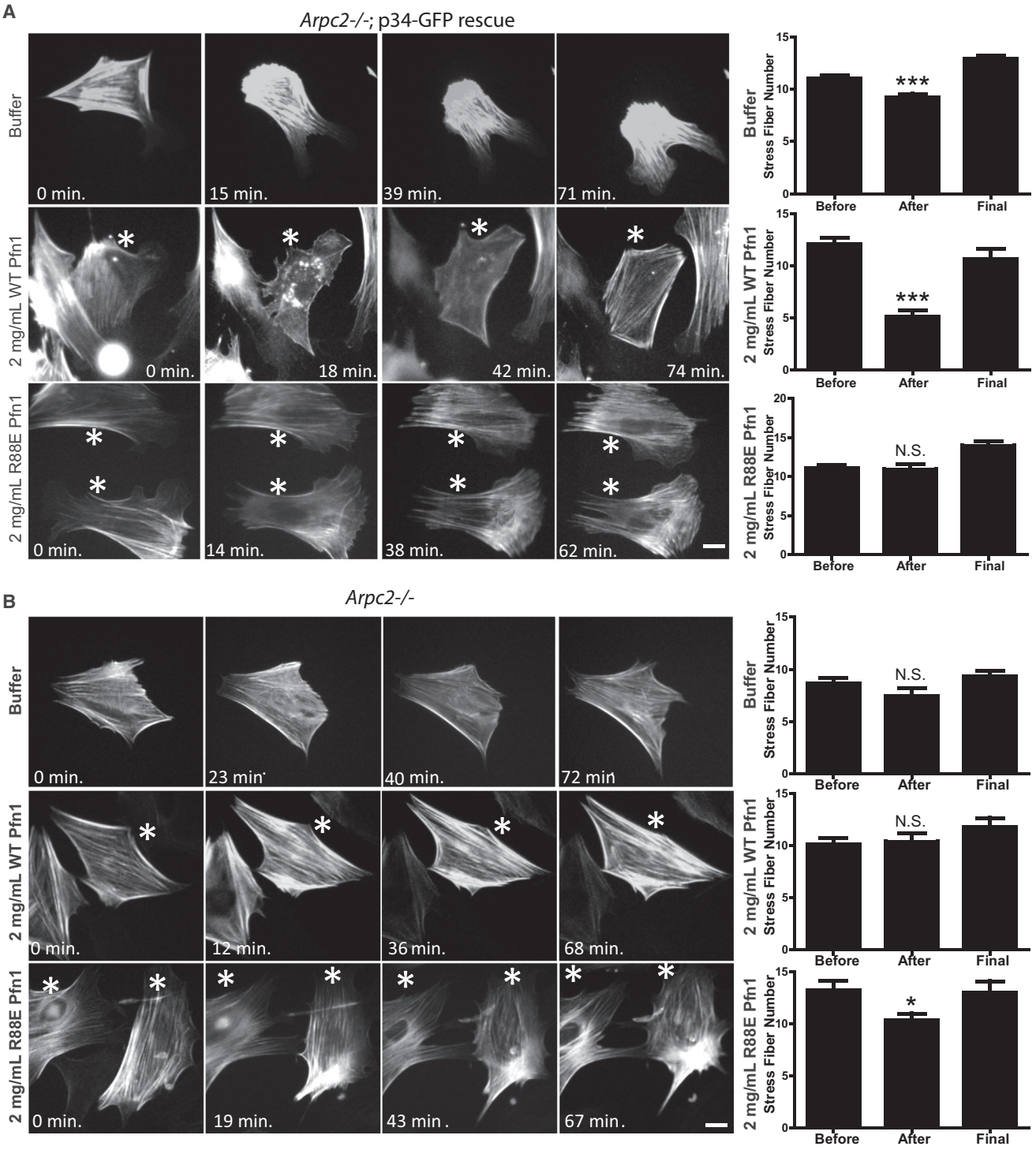

Figure 5. Profilin Affects Overall F-Actin Structure in Cells with Functional Arp2/3 Complex

(A) Representative images of Lifeact-RFP labeling in p34 knockout-rescue cells (*Arpc2*$^{-/-}$; p34-GFP rescue) before (0 min.) and at various times after microinjection of buffer, 2 mg/ml WT hProfilin-1, or 2 mg/ml R88E hProfilin-1. Scale bar, 20 μm. Asterisks denote microinjected cells in images with multiple cells. Right: Quantification of stress fiber number from images before, after, and at the end (Final) of the postinjection time course. Counted as number of stress fibers across a line drawn perpendicular to the predominant stress fiber orientation, plotted as mean with SEM; N = 198 measurements from 66 buffer-injected cells, 78 measurements from 26 WT hProfilin-1 injected cells, or 60 measurements from 20 R88E hProfilin-1 injected cells. ***$p < 0.0001$. N.S., not significant.

(legend continued on next page)

key effects of profilin-1 depletion in the same cells. Together, these data suggest that mammalian cells maintain F-actin homeostasis in the absence of Arp2/3 complex by activating profilin-1-dependent and Ena/VASP-dependent actin assembly.

DISCUSSION

In this work, we utilized cell lines isolated from a conditional knockout mouse in the *Arpc2* gene encoding the p34 subunit of the Arp2/3 complex to interrogate F-actin dynamics, organization, and homeostasis in the presence or absence of the Arp2/3 complex. We found, as in previous studies (Suraneni et al., 2012; Wu et al., 2012), that cells lacking the Arp2/3 complex possessed filopodial protrusions containing bundled actin filaments, lacked lamellipodia, migrated slowly, and had less dynamic actin networks than control cells. Surprisingly, we found that *Arpc2*$^{-/-}$ cells could compensate for loss of Arp2/3 complex and maintain overall F-actin levels similar to control cells. In addition, *Arpc2*$^{-/-}$ cells are resistant to low doses of CD and require profilin-1 and Ena/VASP, but not formins, to maintain proper levels of F-actin. Finally, consistent with previous biochemical studies, our data reveal an important role for profilin-1 in inhibiting Arp2/3 complex function in mammalian cells. Together, these observations suggest that profilin-1 plays a major gatekeeper role in actin assembly by directing actin monomers toward formin and Ena/VASP pathways and away from Arp2/3-based actin assembly.

Profilin-actin is thought to be the major form of monomeric actin in cells (Kaiser et al., 1999). Our data identify a critical role for profilin-1 in maintaining F-actin levels in the absence of Arp2/3 complex. Formins and Ena/VASP associate with filament barbed ends and act as actin polymerases that elongate actin filaments while protecting barbed ends from capping (Bear et al., 2002; Breitsprecher and Goode, 2013; Hansen and Mullins, 2010; Winkelman et al., 2014). Our experiments yielded the surprising finding that formins did not appear to contribute significantly to global F-actin maintenance in *Arpc2*$^{-/-}$ cells. The fact that formin inhibition did not affect the F-actin organization and content of the *Arpc2*$^{-/-}$ cells is surprising given the key role that formins play in compensating for the loss of Arp2/3 complex activity in fission yeast (Burke et al., 2014). However, yeast cells do not have proteins homologous to Ena/VASP, and recent data in insect cells indicate that Ena/VASP proteins and formins do not merely substitute for each other functionally but have a more complex interaction than previously suspected (Bilancia et al., 2014). Our data in mammalian cells indicate that Ena/VASP proteins play a major role in compensating for the loss of Arp2/3 complex when it comes to maintaining overall F-actin levels. It will be important to revisit the issue of the relative contribution of Ena/VASP and formins to both specific actin structures and overall F-actin levels as reagents to perturb formins in mammalian systems continue to improve.

In addition to being described as anticapping factors, Ena/VASP proteins have also been described as "anti-branching" factors (Bear and Gertler, 2009). FP4-mito expression, which blocks Ena/VASP function, leads to increased actin filament branching and decreased filament length at the leading edge, whereas targeting of Ena/VASP proteins to the membrane gives rise to a converse phenotype, implying Arp2/3 complex inhibition by Ena/VASP (Bear et al., 2002). Additionally, ActA-induced Arp2/3 complex nucleation is inhibited in the presence of VASP (Skoble et al., 2001). Two possible mechanisms for the proposed "antibranching" activity of Ena/VASP are (1) direct inhibition of Arp2/3 complex by Ena/VASP and (2) indirect inhibition via competition for actin monomers. We find in TIRF microscopy assays that the presence of VASP alone does not affect Arp2/3 complex nucleation, arguing against direct inhibition. Ena/VASP's "antibranching" activity in cells may relate to its recruitment of profilin-actin that cannot be used by the Arp2/3 complex for branch nucleation. It is already known that profilin enhances, but is not required for, Ena/VASP's anticapping activity (Barzik et al., 2005). Future experiments will be required to clarify the relationship between Ena/VASP, profilin-1, and the Arp2/3 complex and whether "antibranching" is a distinct mechanism from anticapping. However, this matter may be even more complicated, given the recent finding that VASP can bind to and positively regulate the WAVE regulatory complex via Abi-1 and, therefore, Arp2/3 complex activity (Chen et al., 2014).

One of the most important findings in this work is the inhibitory role that profilin-1 plays in Arp2/3-dependent actin assembly pathways in cells. Decreasing profilin-1 (via RNAi) and increasing profilin-1 (via microinjection) levels led to reciprocal changes in Arp2/3 complex activity, as evidenced by leading edge incorporation and lamellipodia formation. In fact, the relationship between the Arp2/3 complex and profilin-1 appears to be precisely balanced, a balance that can be shifted even by modest changes in their relative levels. While these findings establish an inhibitory activity for profilin-1 toward the Arp2/3 complex in mammalian cells, prior biochemical studies showed profilin inhibition of Arp2/3 complex nucleation in vitro (Machesky et al., 1999; Rodal et al., 2003). Direct observation of Arp2/3 complex branch formation in vitro using purified mammalian proteins yielded the important observation that profilin decreased Arp2/3 complex branching while increasing filament length (Blanchoin et al., 2000), similar to experiments reported in our study as well as in Suarez et al. (2015).

Our data confirm and extend these in vitro findings, but there are several mechanistic possibilities that are worth considering about the inhibitory effect of profilin toward Arp2/3 complex, which could be either direct or indirect. The Arp2/3 complex was initially discovered and characterized as a profilin-binding complex from *Acanthamoeba* (Machesky et al., 1994; Mullins et al., 1998). Though the affinity of the interaction is relatively low (K_D = 7 μM) (Mullins et al., 1998), a direct protein-protein interaction could allosterically inhibit Arp2/3 complex activity or block recruitment of NPFs to the complex. The structure/function and mutagenesis experiments required to test this

(B) Representative images of LA-RFP labeling in *Arpc2*$^{-/-}$ cells before (0 min.) and at various times after microinjection of buffer, 2 mg/ml WT hProfilin-1, or 2 mg/ml R88E hProfilin-1. Scale bar, 20 μm. Asterisks denote microinjected cells in images with multiple cells. Right: Quantification of stress fiber number, plotted as mean with SEM; N = 36 measurements from 12 buffer-injected cells, 60 measurements from 20 WT hProfilin-1 injected cells, or 42 measurements from 14 R88E hProfilin-1 injected cells. *p = 0.0103.
See also Figure S3.

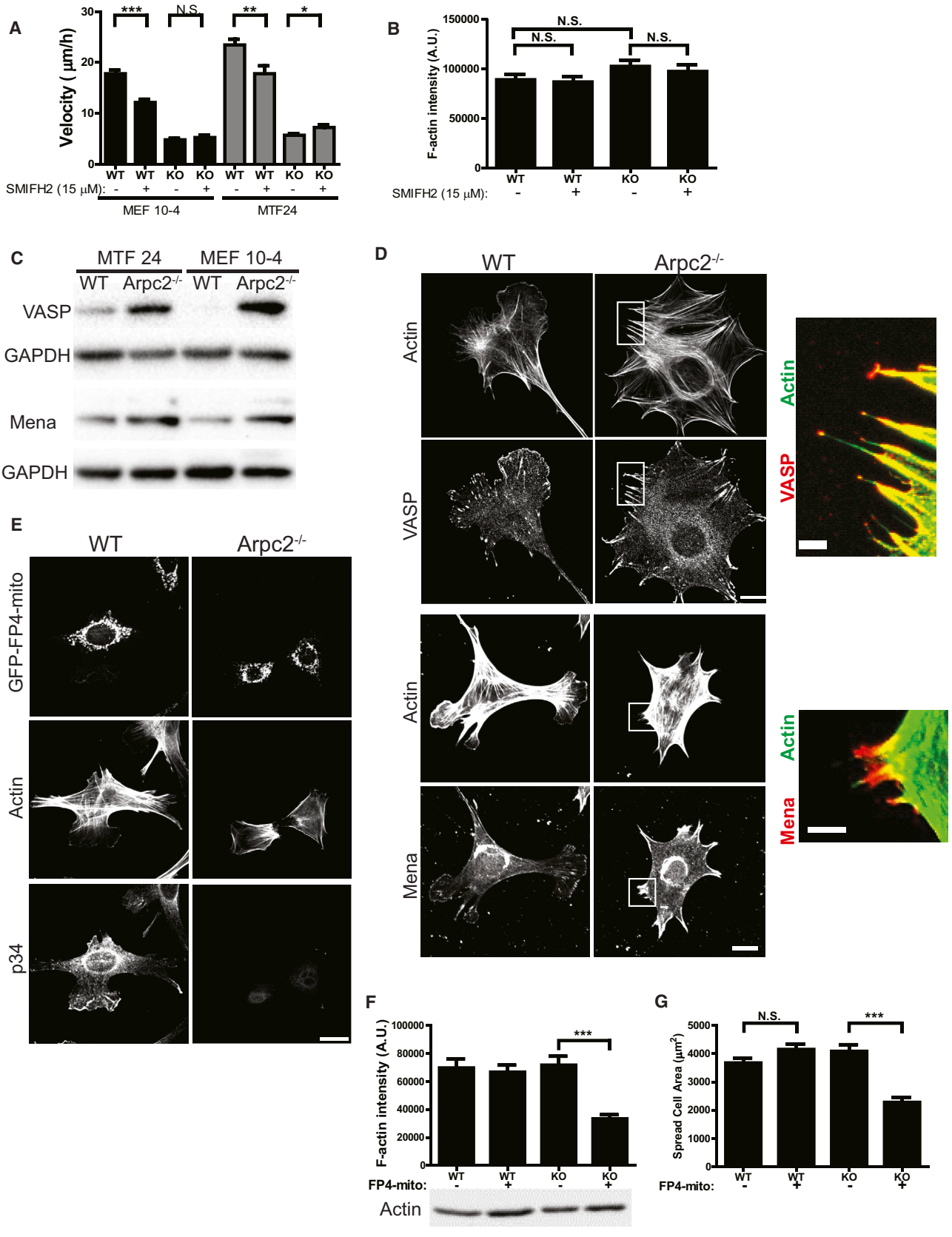

(legend on next page)

interesting possibility conclusively lie outside the scope of the present effort.

Both our work and the accompanying paper from Suarez et al. (2015) support the idea of indirect inhibition of Arp2/3 complex by profilin through competition for actin monomers. Both groups show that profilin mutants (R88E or K81E, respectively) with greatly reduced affinity for G-actin do not inhibit Arp2/3 complex branch generation in vitro. Our microinjection studies also show reduced ability of this mutant to inhibit Arp2/3-containing lamellipodia, although the effect is less clear cut than the in vitro studies. One possible explanation for this partial effect of the R88E mutant in vivo is that this mutant may act as a dominant-negative mutant for the formin and Ena/VASP pathways, which are known to contribute to lamellipodia formation (Yang et al., 2007). Furthermore, Suarez et al. (2015) directly demonstrate competition between fission yeast profilin and WASP (VCA) for actin monomers in vitro. In cells, according to this model, profilin-actin preferentially delivers actin monomers to Ena/VASP and formins, whereas NPFs deliver actin monomers to the Arp2/3 complex for nucleation of daughter filaments. It is known that the affinity of VCA and profilin for G-actin is similar (Marchand et al., 2001). Despite the high cellular concentrations of profilin (Kaiser et al., 1999; Tseng et al., 1984), it is also known that nanomolar VCA/NPF concentrations can maintain lower but observable Arp2/3 complex activity in the presence of saturating (in micromolar) profilin concentrations (Blanchoin et al., 2000; Machesky et al., 1999; Rodal et al., 2003). In future studies, it will be interesting to test whether known profilin regulatory mechanisms such as PIP_2 binding and/or tyrosine phosphorylation (Ding et al., 2012; Fan et al., 2012) can tip the balance between Arp2/3-dependent and -independent actin assembly pathways. Our results suggest that disruption of any aspect of actin regulation will lead to a resulting compensation (or defect) that reveals functional connections and interplay occurring in normal cells. Physiological cues and cellular context will certainly help determine the regulatory interplay between these pathways during cellular events such as vesicular trafficking, migration, and adhesion.

EXPERIMENTAL PROCEDURES

A complete description of all experimental procedures can be found in the Supplemental Information.

Mouse Strains

C57BL/6 mice with conditional *Arpc2* alleles were ordered from the European Conditional Mouse Mutagenesis Program consortium, mated to FLP recombinase mice, and were then crossed with previously established *Ink4a/Arf*$^{-/-}$ mice (in a mixed genetic background; mice were null for both Ink4a and Arf) (Serrano et al., 1996) and homozygosed to generate p34$^{FL/FL}$; *Ink4a/Arf*$^{-/-}$ mice in a mixed strain background. All mouse experiments were reviewed and approved by the University of North Carolina at Chapel Hill Institutional Animal Care and Use Committee and were provided with food and water ad libitum.

F-Actin and Total Actin Quantitation

After coverslips were processed according to standard lab protocol (reported in depth in the Supplemental Experimental Procedures), images were taken on an Olympus IX81 microscope with a 0.30 NA 10× objective and an iXon+ front-illuminated EMCCD camera (Andor Technology) and controlled by MetaMorph software (Molecular Devices). Images of fluorescent phalloidin were used to determine F-actin content. Briefly, image files were imported into ImageJ, and background was subtracted by the program. Cells were carefully outlined by hand, and integrated pixel density was measured on a per-cell basis to generate average F-actin content per cell. Measurements of the area of outlined cells were generated, and subsequently reported as average spread cell area. As cells were plated for F-actin visualization, a subset of trypsinized cells of the same population (matched at 25,000 cells per condition) were spun down at 1,000 × g for 3 min at room temperature, and whole cell lysates were prepared from pelleted cells. Ten microliters of whole cell lysate was used per sample on SDS-PAGE gels. Actin and p34 signal from whole cell lysate was simultaneously detected with Li-Cor fluorescent antibodies on an Odyssey detection system (Li-Cor).

Single-Molecule TIRF

Full experimental conditions can be found in the Supplemental Experimental Procedures. TIRF microscopy images were collected at 5 s intervals with an iXon EMCCD camera (Andor Technology) using an Olympus IX-71 microscope equipped with through-the-objective TIRF microscopy illumination. Elongation rates were measured using ImageJ, and branch densities were calculated by counting the number of branch points and dividing by the total filament length.

Microinjection

Cells were plated overnight in low CO_2 adjustment media on Delta-T dishes (Bioptechs) and sealed with parafilm. Cells were removed the next morning and placed into a heated insert for imaging on an Olympus IX81 microscope with a 1.05 NA 30× silicon oil objective and an iXon+ front-illuminated EMCCD camera (Andor Technology) and controlled by MetaMorph software (Molecular Devices). Several cells were imaged in the GFP, RFP, and Cy5 channels prior to microinjection, and stage positions were saved. Saved positions were then revisited for microinjection. Microinjection with Femtotip needles was accomplished with the FemtoJet injection controller and InjectMan NI 2 system (Eppendorf). Needles were loaded with 2 mg/ml (133 μM) WT or R88E human profilin in profilin buffer (20 mM Tris [pH 7.5]; 150 mM KCl; 0.2 mM dithiothreitol) plus 0.67 μg/ml Cy5-conjugated dextran (Sigma), or buffer and dextran alone. Using a standard curve of purified His-profilin-1 (Cytoskeleton), we determined the average level of profilin-1 in 2,500 cells to be ~5 ng. The corresponding level per cell is 2 pg or 133.33 amol profilin-1. We imaged cells in suspension and found them to have an average cytoplasmic volume of 4.6 pl. Based on

Figure 6. Formin and Ena/VASP Differentially Affect Actin Homeostasis Depending on Cellular Arp2/3 Complex Status

(A) Random migration velocity of MEF 10-4 (black bars) and MTF24 (gray bars) WT and KO control (–) cells or cells treated with 15 μM SMIFH2 (+), plotted as mean and SEM; N = at least 48 cells per condition. *p = 0.0219; **p = 0.0040; ***p < 0.0001. N.S., not significant. h, hours.

(B) Integrated pixel density of phalloidin staining in fixed MEF 10-4 WT and KO cells in the presence or absence of 15 μM SMIFH2, plotted as average F-actin intensity per cell, with SEM. N = at least 120 cells per condition. A.U., arbitrary units.

(C) Blots of WT and *Arpc2*$^{-/-}$ cells.

(D) Staining of MEF 10-4 WT and *Arpc2*$^{-/-}$ fibroblasts; scale bar, 20 μm. Boxed regions are magnified and merged with VASP or Mena in red and F-actin in green; scale bar of magnified image is 5 μm.

(E) Staining of MEF 10-4 WT and *Arpc2*$^{-/-}$ cells expressing GFP-FP4-mito. Scale bar, 20 μm.

(F) Integrated pixel density of phalloidin staining in fixed MEF 10-4 WT and KO cells, or WT/KO cells stably expressing GFP-FP4-mito (FP4-mito +), plotted as average F-actin intensity per cell, with SEM. N = at least 38 cells per condition. ***p < 0.0001. Blots of whole cell lysate matched by cell number directly below.

(G) Spread cell area in square microns of MEF 10-4 WT, WT FP4-mito, KO, and KO FP4-mito cells plotted as average area per cell with SEM. N = at least 140 cells per condition; ***p < 0.0001.

See also Figures S4–S6.

these values, we calculated a cellular profilin-1 concentration of ~29 μM, in line with published values in mammalian cells that range from 8.4 to 50 μM (Finkel et al., 1994; Goldschmidt-Clermont et al., 1991). Though microinjected volume likely differed from cell to cell, the manufacturer's data regarding their Femtotip needle reported an injection range of 0.1–0.5 pl. As 0.5 pl is ~10% of cell volume, we find it reasonable as an upper bound for injection volume. Given this and the needle concentration of profilin, we could deliver 1 pg (66.67 amol) of profilin. The postinjection concentration of profilin-1 would be 39 μM, an immediate 36% increase in profilin-1 levels. After microinjection, cells were allowed to re-equilibrate until Z drift was minimized. Cells at each saved position were imaged every 8 min on GFP, RFP, and Cy5 channels.

Image Analysis

Actin and Arp2/3 Complex Edge Detection

The ImageJ macro EdgeRatio (http://www.unc.edu/~cail/code/EdgeRatio.txt) (Cai et al., 2007) was used to measure the distribution of F-actin and p34Arc at the cell edge. A full description of this analysis method can be found in the Supplemental Experimental Procedures.

In Situ Actin Assembly Quantification

F-actin and Alexa Fluor 488-actin signal was background subtracted, cells were outlined, and fluorescence of both channels was quantified in ImageJ. Barbed-end intensity was normalized to total F-actin. Averages of normalized values are reported relative to control WT cells minus profilin.

Arp2/3 Complex Edge Ratio

Confocal stacks of cells imaged on an Olympus FV1000 microscope at 40× were analyzed using MATLAB (MathWorks). Cells were automatically segmented from background via k-means clustering. High Arp2/3 complex signal (designated as intensity greater than 1.2 SD above the mean signal for the whole cell) was analyzed within a five-pixel band along the cell perimeter. Perimeter area covered by high Arp2/3 complex signal was divided by the total perimeter area of the cell to achieve the final fraction of Arp2/3 complex-enriched edge.

Actin Stress Fiber Quantification

Analysis was done in a manner similar to that of already established approaches (Wei et al., 2011). A full description can be found in the Supplemental Experimental Procedures.

Peripheral Lamellipodia Length

p34-positive lamellipodia length was analyzed in ImageJ by hand drawing a curved line on top of p34-positive lamellipodial regions. The length of the curved line in microns was measured using the ImageJ software.

Statistical Analysis

All means are graphed with SEM, with the exception of barbed-end quantification in which error bars represent 95% confidence intervals. Statistical significance was assessed using unpaired two-tailed t tests, with p values < 0.05 being considered significant. All statistical tests of raw data were conducted in GraphPad Prism (GraphPad Software).

SUPPLEMENTAL INFORMATION

Supplemental Information includes Supplemental Experimental Procedures, six figures, and two movies and can be found with this article online at http://dx.doi.org/10.1016/j.devcel.2014.10.026.

AUTHOR CONTRIBUTIONS

J.D.R. and C.W. designed and performed experiments, analyzed data, and wrote the paper; E.M.H. analyzed data; J.D.W. and C.S. performed and analyzed TIRF experiments and wrote associated methodological text; H.E.J. and J.M.H. developed the Arp2/3 complex edge ratio MATLAB application; D.R.K. proposed and directed TIRF experiments; J.E.B. proposed and designed experiments, analyzed data, and wrote the paper. All authors reviewed and made comments on the manuscript before publication.

ACKNOWLEDGMENTS

This work was supported by NIH grants to J.E.B. (GM111557) and D.R.K. (GM079265), a National Science Foundation grant to J.M.H. (1133476), and support from the Howard Hughes Medical Institute to J.E.B. We thank Jack D. Griffith and the Lineberger Electron Microscopy core for assistance with cryoshadowing EM experiments, and Tao Bo for technical assistance with mouse husbandry and dissection, and members of our laboratories for critical reading of the manuscript.

Received: April 7, 2014
Revised: September 12, 2014
Accepted: October 30, 2014
Published: December 24, 2014

REFERENCES

Barzik, M., Kotova, T.I., Higgs, H.N., Hazelwood, L., Hanein, D., Gertler, F.B., and Schafer, D.A. (2005). Ena/VASP proteins enhance actin polymerization in the presence of barbed end capping proteins. J. Biol. Chem. *280*, 28653–28662.

Bear, J.E., and Gertler, F.B. (2009). Ena/VASP: towards resolving a pointed controversy at the barbed end. J. Cell Sci. *122*, 1947–1953.

Bear, J.E., Loureiro, J.J., Libova, I., Fässler, R., Wehland, J., and Gertler, F.B. (2000). Negative regulation of fibroblast motility by Ena/VASP proteins. Cell *101*, 717–728.

Bear, J.E., Svitkina, T.M., Krause, M., Schafer, D.A., Loureiro, J.J., Strasser, G.A., Maly, I.V., Chaga, O.Y., Cooper, J.A., Borisy, G.G., and Gertler, F.B. (2002). Antagonism between Ena/VASP proteins and actin filament capping regulates fibroblast motility. Cell *109*, 509–521.

Bilancia, C.G., Winkelman, J.D., Tsygankov, D., Nowotarski, S.H., Sees, J.A., Comber, K., Evans, I., Lakhani, V., Wood, W., Elston, T.C., et al. (2014). Enabled negatively regulates diaphanous-driven actin dynamics in vitro and in vivo. Dev. Cell *28*, 394–408.

Blanchoin, L., Amann, K.J., Higgs, H.N., Marchand, J.B., Kaiser, D.A., and Pollard, T.D. (2000). Direct observation of dendritic actin filament networks nucleated by Arp2/3 complex and WASP/Scar proteins. Nature *404*, 1007–1011.

Breitsprecher, D., and Goode, B.L. (2013). Formins at a glance. J. Cell Sci. *126*, 1–7.

Burke, T.A., Christensen, J.R., Barone, E., Suarez, C., Sirotkin, V., and Kovar, D.R. (2014). Homeostatic actin cytoskeleton networks are regulated by assembly factor competition for monomers. Curr. Biol. *24*, 579–585.

Cai, L., Marshall, T.W., Uetrecht, A.C., Schafer, D.A., and Bear, J.E. (2007). Coronin 1B coordinates Arp2/3 complex and cofilin activities at the leading edge. Cell *128*, 915–929.

Campellone, K.G., and Welch, M.D. (2010). A nucleator arms race: cellular control of actin assembly. Nat. Rev. Mol. Cell Biol. *11*, 237–251.

Cao, L.G., Babcock, G.G., Rubenstein, P.A., and Wang, Y.L. (1992). Effects of profilin and profilactin on actin structure and function in living cells. J. Cell Biol. *117*, 1023–1029.

Chen, X.J., Squarr, A.J., Stephan, R., Chen, B., Higgins, T.E., Barry, D.J., Martin, M.C., Rosen, M.K., Bogdan, S., and Way, M. (2014). Ena/VASP proteins cooperate with the WAVE complex to regulate the actin cytoskeleton. Dev. Cell *30*, 569–584.

Chesarone, M.A., and Goode, B.L. (2009). Actin nucleation and elongation factors: mechanisms and interplay. Curr. Opin. Cell Biol. *21*, 28–37.

Cooper, J.A. (1987). Effects of cytochalasin and phalloidin on actin. J. Cell Biol. *105*, 1473–1478.

Ding, Z., Bae, Y.H., and Roy, P. (2012). Molecular insights on context-specific role of profilin-1 in cell migration. Cell Adhes. Migr. *6*, 442–449.

Evangelista, M., Pruyne, D., Amberg, D.C., Boone, C., and Bretscher, A. (2002). Formins direct Arp2/3-independent actin filament assembly to polarize cell growth in yeast. Nat. Cell Biol. *4*, 260–269.

Fan, Y., Arif, A., Gong, Y., Jia, J., Eswarappa, S.M., Willard, B., Horowitz, A., Graham, L.M., Penn, M.S., and Fox, P.L. (2012). Stimulus-dependent phosphorylation of profilin-1 in angiogenesis. Nat. Cell Biol. *14*, 1046–1056.

Finkel, T., Theriot, J.A., Dise, K.R., Tomaselli, G.F., and Goldschmidt-Clermont, P.J. (1994). Dynamic actin structures stabilized by profilin. Proc. Natl. Acad. Sci. USA *91*, 1510–1514.

Gao, L., and Bretscher, A. (2008). Analysis of unregulated formin activity reveals how yeast can balance F-actin assembly between different microfilament-based organizations. Mol. Biol. Cell *19*, 1474–1484.

Goldschmidt-Clermont, P.J., Machesky, L.M., Doberstein, S.K., and Pollard, T.D. (1991). Mechanism of the interaction of human platelet profilin with actin. J. Cell Biol. *113*, 1081–1089.

Hansen, S.D., and Mullins, R.D. (2010). VASP is a processive actin polymerase that requires monomeric actin for barbed end association. J. Cell Biol. *191*, 571–584.

Hotulainen, P., and Lappalainen, P. (2006). Stress fibers are generated by two distinct actin assembly mechanisms in motile cells. J. Cell Biol. *173*, 383–394.

Kaiser, D.A., Vinson, V.K., Murphy, D.B., and Pollard, T.D. (1999). Profilin is predominantly associated with monomeric actin in Acanthamoeba. J. Cell Sci. *112*, 3779–3790.

Kovar, D.R., Harris, E.S., Mahaffy, R., Higgs, H.N., and Pollard, T.D. (2006). Control of the assembly of ATP- and ADP-actin by formins and profilin. Cell *124*, 423–435.

Lanier, L.M., Gates, M.A., Witke, W., Menzies, A.S., Wehman, A.M., Macklis, J.D., Kwiatkowski, D., Soriano, P., and Gertler, F.B. (1999). Mena is required for neurulation and commissure formation. Neuron *22*, 313–325.

Machesky, L.M., Atkinson, S.J., Ampe, C., Vandekerckhove, J., and Pollard, T.D. (1994). Purification of a cortical complex containing two unconventional actins from Acanthamoeba by affinity chromatography on profilin-agarose. J. Cell Biol. *127*, 107–115.

Machesky, L.M., Mullins, R.D., Higgs, H.N., Kaiser, D.A., Blanchoin, L., May, R.C., Hall, M.E., and Pollard, T.D. (1999). Scar, a WASp-related protein, activates nucleation of actin filaments by the Arp2/3 complex. Proc. Natl. Acad. Sci. USA *96*, 3739–3744.

Marchand, J.B., Kaiser, D.A., Pollard, T.D., and Higgs, H.N. (2001). Interaction of WASP/Scar proteins with actin and vertebrate Arp2/3 complex. Nat. Cell Biol. *3*, 76–82.

Mullins, R.D., Kelleher, J.F., Xu, J., and Pollard, T.D. (1998). Arp2/3 complex from Acanthamoeba binds profilin and cross-links actin filaments. Mol. Biol. Cell *9*, 841–852.

Reinhard, M., Halbrügge, M., Scheer, U., Wiegand, C., Jockusch, B.M., and Walter, U. (1992). The 46/50 kDa phosphoprotein VASP purified from human platelets is a novel protein associated with actin filaments and focal contacts. EMBO J. *11*, 2063–2070.

Rizvi, S.A., Neidt, E.M., Cui, J., Feiger, Z., Skau, C.T., Gardel, M.L., Kozmin, S.A., and Kovar, D.R. (2009). Identification and characterization of a small molecule inhibitor of formin-mediated actin assembly. Chem. Biol. *16*, 1158–1168.

Rodal, A.A., Manning, A.L., Goode, B.L., and Drubin, D.G. (2003). Negative regulation of yeast WASp by two SH3 domain-containing proteins. Curr. Biol. *13*, 1000–1008.

Romero, S., Le Clainche, C., Didry, D., Egile, C., Pantaloni, D., and Carlier, M.F. (2004). Formin is a processive motor that requires profilin to accelerate actin assembly and associated ATP hydrolysis. Cell *119*, 419–429.

Rotty, J.D., Wu, C., and Bear, J.E. (2013). New insights into the regulation and cellular functions of the ARP2/3 complex. Nat. Rev. Mol. Cell Biol. *14*, 7–12.

Sagot, I., Rodal, A.A., Moseley, J., Goode, B.L., and Pellman, D. (2002). An actin nucleation mechanism mediated by Bni1 and profilin. Nat. Cell Biol. *4*, 626–631.

Serrano, M., Lee, H., Chin, L., Cordon-Cardo, C., Beach, D., and DePinho, R.A. (1996). Role of the INK4a locus in tumor suppression and cell mortality. Cell *85*, 27–37.

Skoble, J., Auerbuch, V., Goley, E.D., Welch, M.D., and Portnoy, D.A. (2001). Pivotal role of VASP in Arp2/3 complex-mediated actin nucleation, actin branch-formation, and Listeria monocytogenes motility. J. Cell Biol. *155*, 89–100.

Spector, I., Shochet, N.R., Blasberger, D., and Kashman, Y. (1989). Latrunculins—novel marine macrolides that disrupt microfilament organization and affect cell growth: I. Comparison with cytochalasin D. Cell Motil. Cytoskeleton *13*, 127–144.

Steffen, A., Faix, J., Resch, G.P., Linkner, J., Wehland, J., Small, J.V., Rottner, K., and Stradal, T.E. (2006). Filopodia formation in the absence of functional WAVE- and Arp2/3-complexes. Mol. Biol. Cell *17*, 2581–2591.

Suarez, C., Carroll, R.T., Burke, T.A., Christensen, J.R., Bestul, A.J., Sees, J.A., James, M.L., Sirotkin, V., and Kovar, D.R. (2015). Profilin regulates F-actin network homeostasis by favoring formin over Arp2/3 complex. Dev. Cell *32*, this issue, 43–53.

Suraneni, P., Rubinstein, B., Unruh, J.R., Durnin, M., Hanein, D., and Li, R. (2012). The Arp2/3 complex is required for lamellipodia extension and directional fibroblast cell migration. J. Cell Biol. *197*, 239–251.

Svitkina, T.M., Bulanova, E.A., Chaga, O.Y., Vignjevic, D.M., Kojima, S., Vasiliev, J.M., and Borisy, G.G. (2003). Mechanism of filopodia initiation by reorganization of a dendritic network. J. Cell Biol. *160*, 409–421.

Symons, M.H., and Mitchison, T.J. (1991). Control of actin polymerization in live and permeabilized fibroblasts. J. Cell Biol. *114*, 503–513.

Tseng, P.C., Runge, M.S., Cooper, J.A., Williams, R.C., Jr., and Pollard, T.D. (1984). Physical, immunochemical, and functional properties of Acanthamoeba profilin. J. Cell Biol. *98*, 214–221.

Wei, S., Gao, X., Du, J., Su, J., and Xu, Z. (2011). Angiogenin enhances cell migration by regulating stress fiber assembly and focal adhesion dynamics. PLoS ONE *6*, e28797.

Winkelman, J.D., Bilancia, C.G., Peifer, M., and Kovar, D.R. (2014). Ena/VASP Enabled is a highly processive actin polymerase tailored to self-assemble parallel-bundled F-actin networks with Fascin. Proc. Natl. Acad. Sci. USA *111*, 4121–4126.

Winter, D.C., Choe, E.Y., and Li, R. (1999). Genetic dissection of the budding yeast Arp2/3 complex: a comparison of the in vivo and structural roles of individual subunits. Proc. Natl. Acad. Sci. USA *96*, 7288–7293.

Wu, C., Asokan, S.B., Berginski, M.E., Haynes, E.M., Sharpless, N.E., Griffith, J.D., Gomez, S.M., and Bear, J.E. (2012). Arp2/3 is critical for lamellipodia and response to extracellular matrix cues but is dispensable for chemotaxis. Cell *148*, 973–987.

Wu, C., Haynes, E.M., Asokan, S.B., Simon, J.M., Sharpless, N.E., Baldwin, A.S., Davis, I.J., Johnson, G.L., and Bear, J.E. (2013). Loss of Arp2/3 induces an NF-κB-dependent, nonautonomous effect on chemotactic signaling. J. Cell Biol. *203*, 907–916.

Yang, C., Czech, L., Gerboth, S., Kojima, S., Scita, G., and Svitkina, T. (2007). Novel roles of formin mDia2 in lamellipodia and filopodia formation in motile cells. PLoS Biol. *5*, e317.